



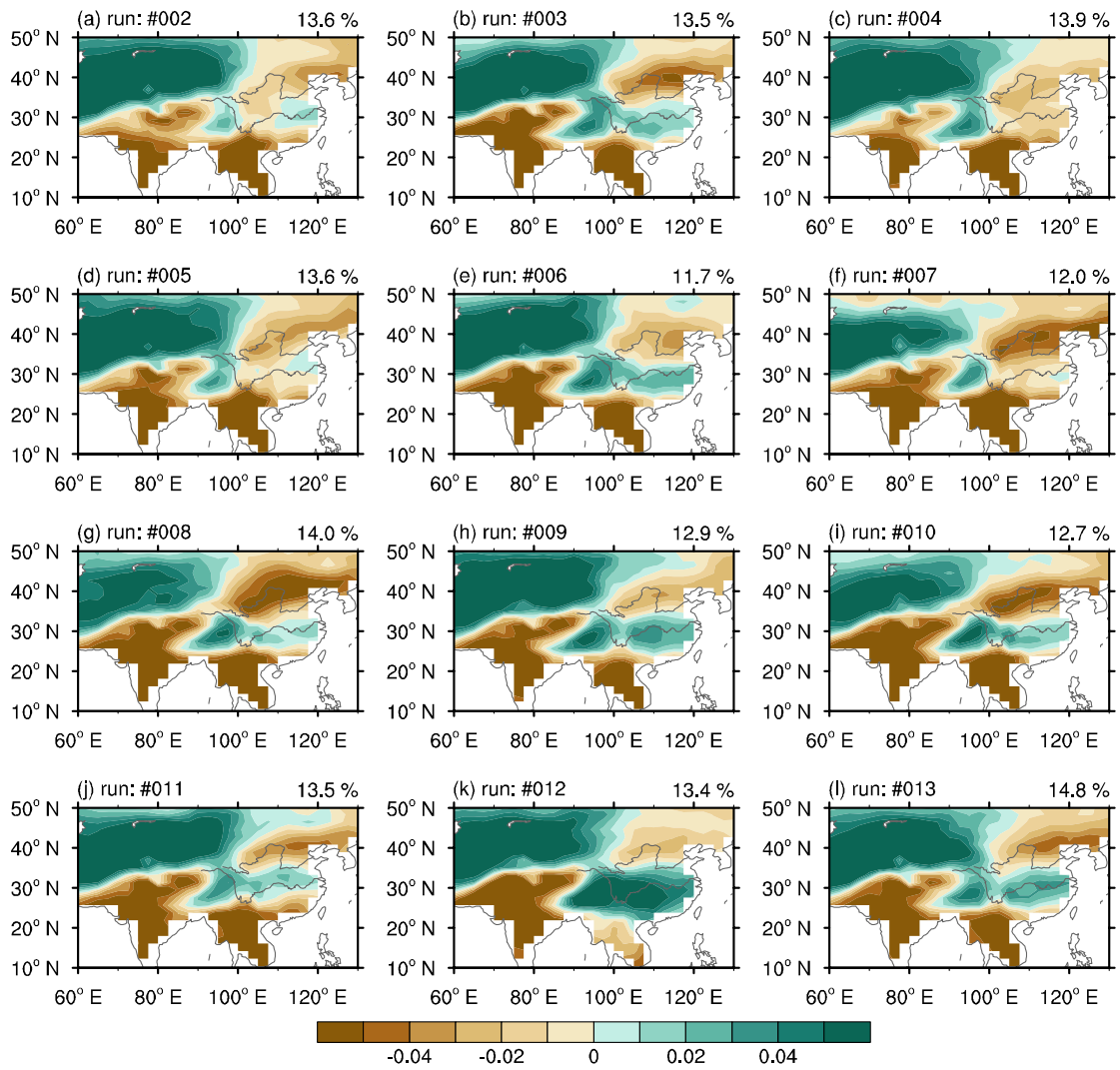
Supplement of

The Interdecadal Pacific Oscillation is responsible for the linkage of decadal changes in precipitation and moisture in arid central Asia and the humid Asian monsoon region during the last millennium

Hongna Xu et al.

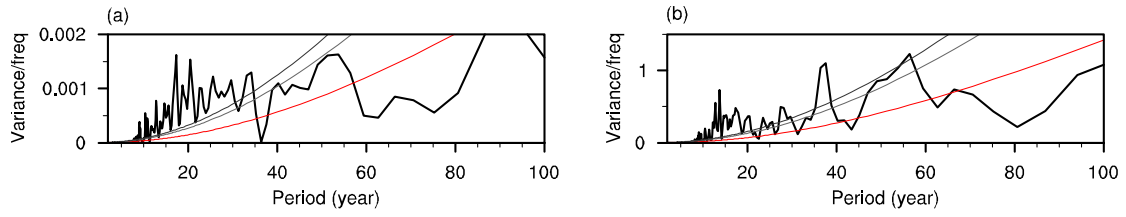
Correspondence to: Tao Wang (wangtao@mail.iap.ac.cn)

The copyright of individual parts of the supplement might differ from the article licence.



1
2
3
4
5

Figure S1. The simulated first leading precipitation mode. (a–l) EOF1 of the nine-year low-pass Lanczos filtered annual precipitation in the CESM-LME 12 all-forcing simulations for the time period 850–2005. The explained variances are given at the top-right.



6

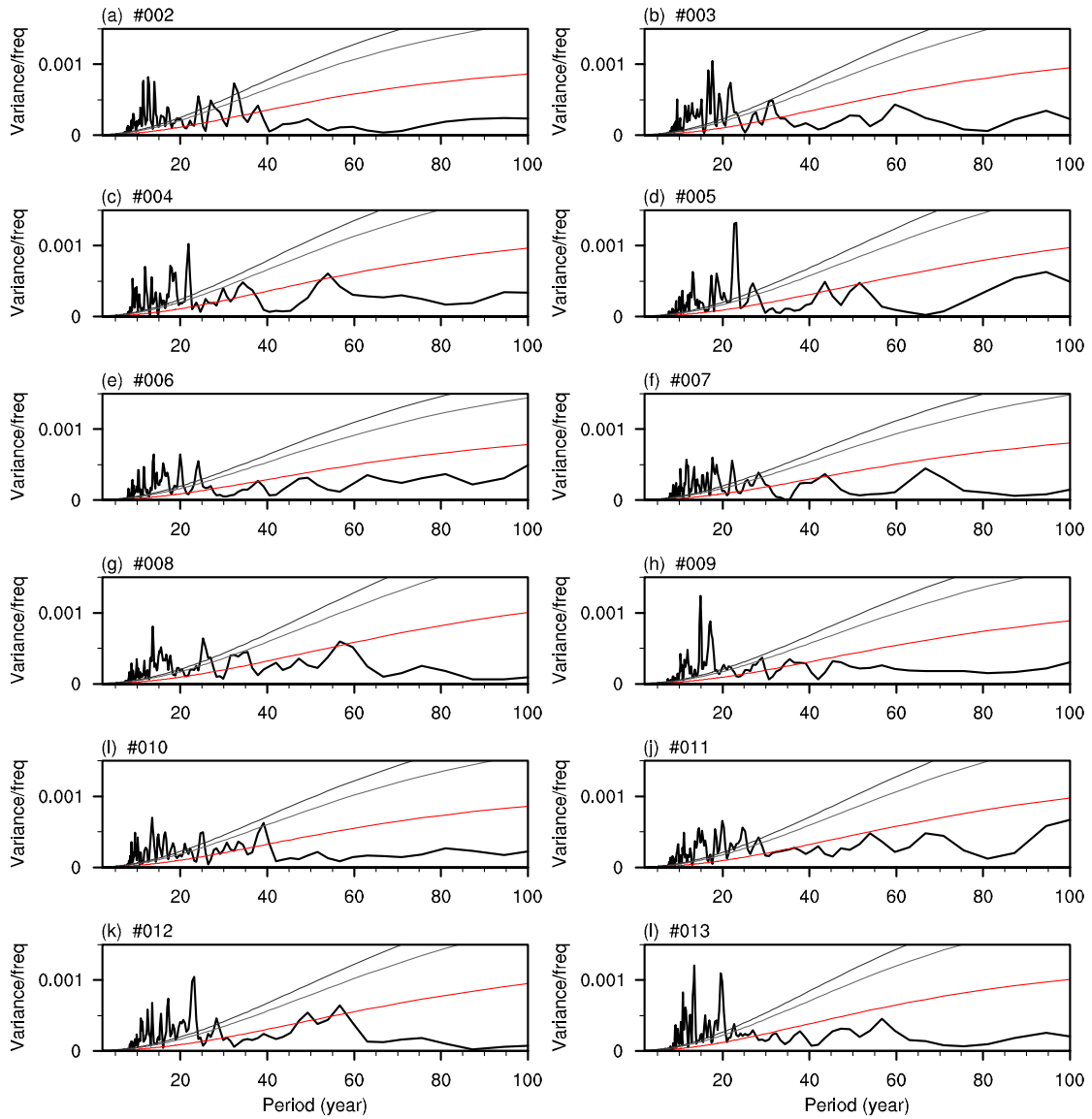
7 **Figure S2. (a)** Power spectrum of the time series of the leading decadal precipitation mode (black

8 line) and **(b)** power spectrum of the time series of the IPO index (black line) in the Last

9 Millennium Reanalysis dataset. The dark (light) gray line indicates the confidence curve at the 95%

10 (90%) confidence level and the red line shows the Markov red noise spectrum.

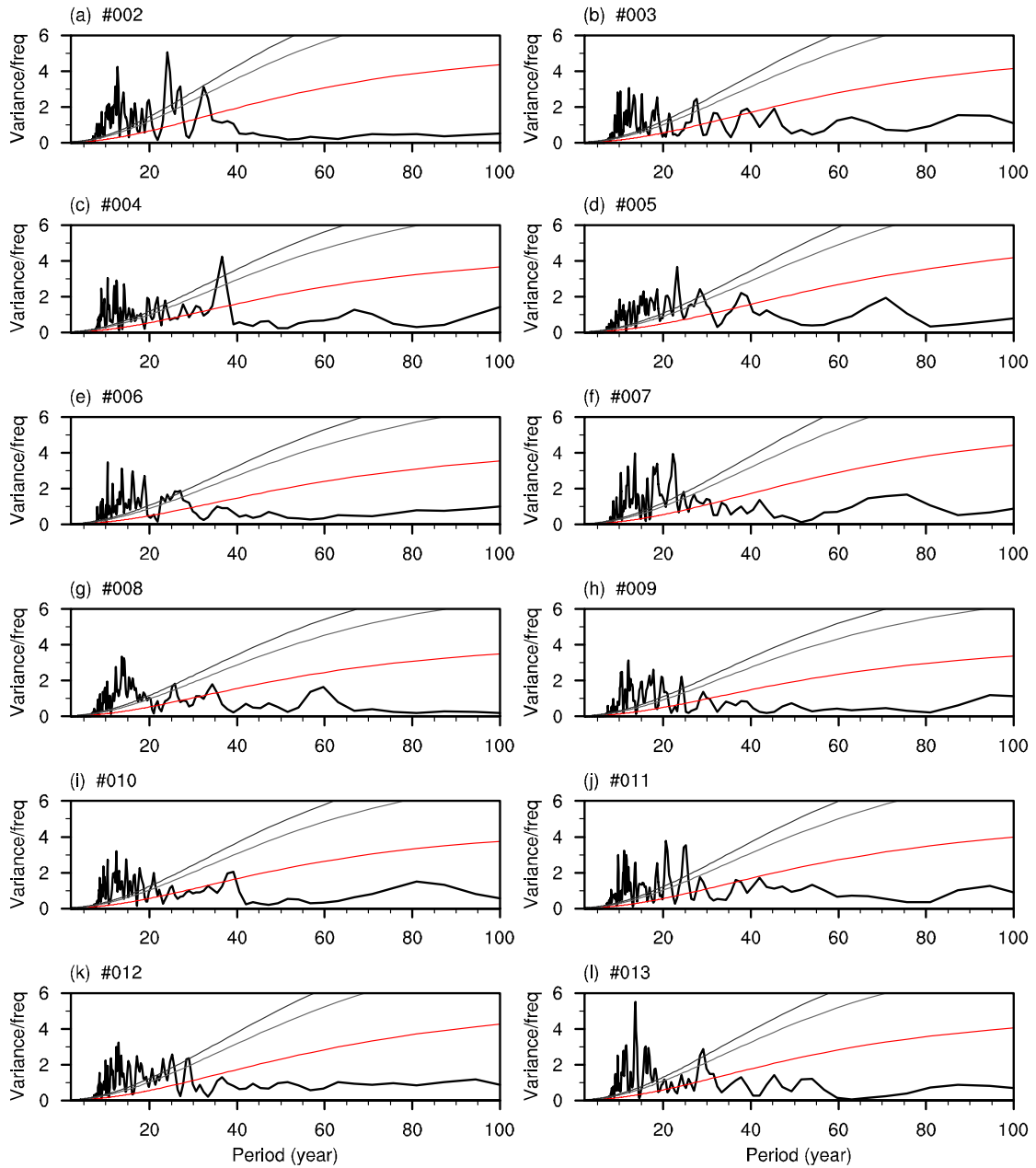
11



12

13 **Figure S3.** Power spectrum of the time series of the leading decadal precipitation mode (black
 14 lines) in the CISM-LME 12 all-forcing simulations. The dark (light) gray lines indicate the
 15 confidence curve at the 95% (90%) confidence level and the red lines show the Markov red noise
 16 spectrum.

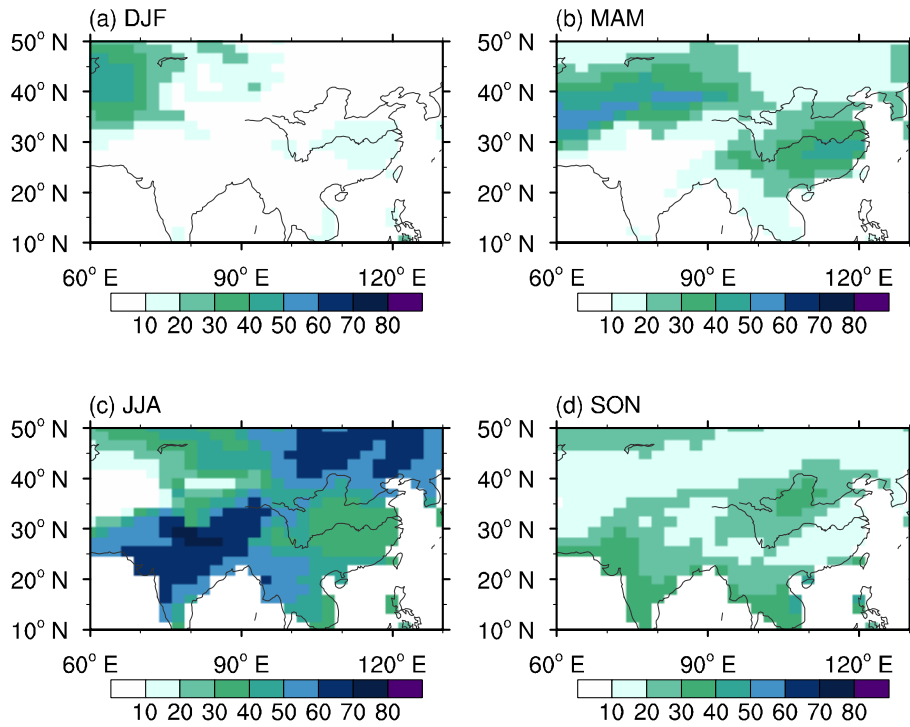
17



18

19 **Figure S4.** Power spectrum of the time series of the IPO index (black lines) in the CESM-LME 12
 20 all-forcing simulations. The dark (light) gray lines indicate the confidence curve at the 95% (90%)
 21 confidence level and the red lines show the Markov red noise spectrum.

22



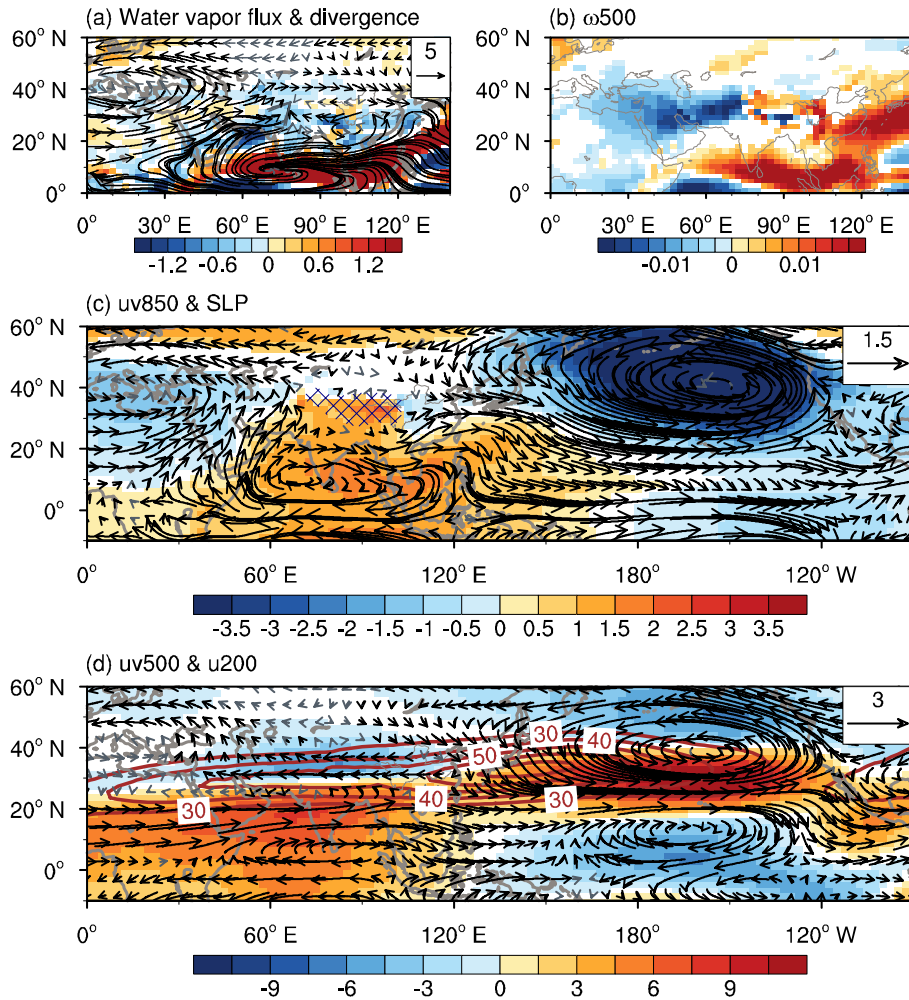
23

24 **Figure S5.** Average values of the percentage of the annual precipitation accounted for by (a)

25 winter, (b) spring, (c) summer and (d) autumn precipitation in the CESM-LME all-forcing

26 simulations.

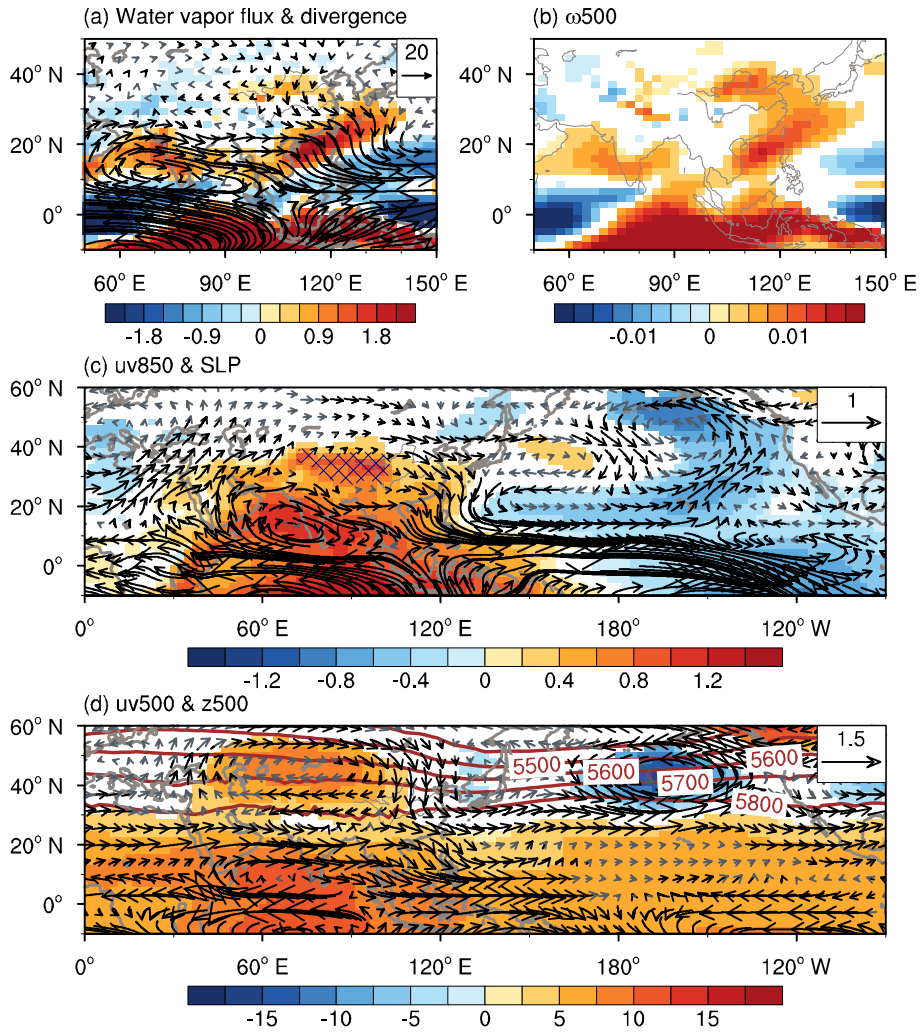
27



28

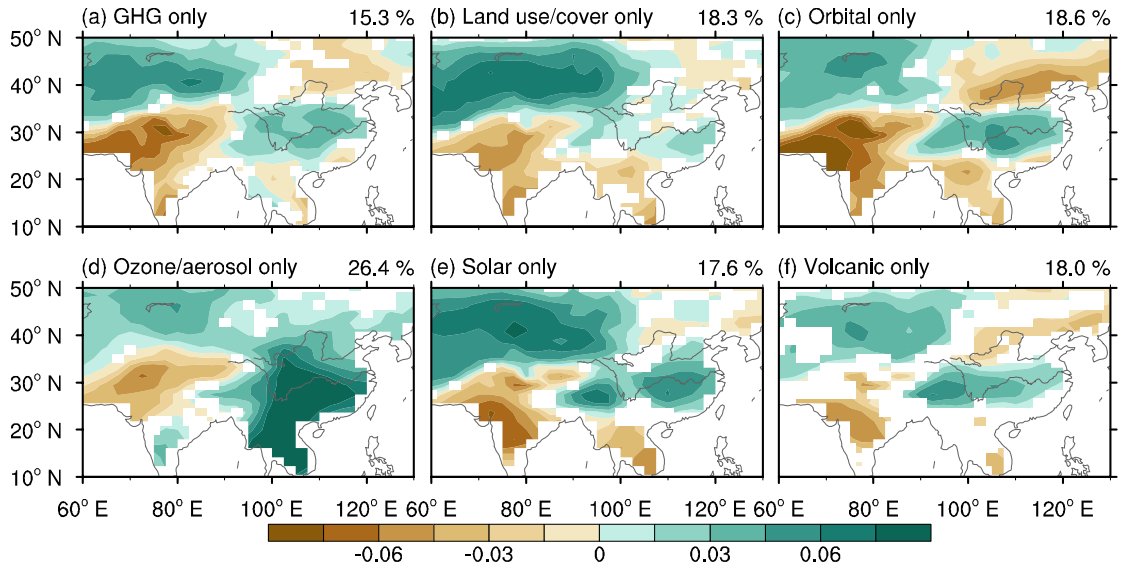
29 **Figure S6.** Simulated winter atmospheric circulation anomalies during the positive phases of the
 30 IPO. Regressed maps of anomalous (a) vertically integrated water vapor flux from 1000 to 300
 31 hPa (vectors; units: $\text{kg m}^{-1} \text{s}^{-1}$) and its divergence (shading; units: $10^{-5} \text{kg m}^{-2} \text{s}^{-1}$), (b) 500 hPa
 32 vertical velocity (ω_{500}) (units: Pa s^{-1}), (c) 850 hPa wind (uv850) (vectors; units: m s^{-1}) and SLP
 33 (shading; units: hPa), (d) 500 hPa wind (uv500) (vectors; units: m s^{-1}) and 200 hPa zonal wind
 34 (u200) (shading; units: m s^{-1}) onto the time series of the IPO index simulated by the CESM-LME
 35 all-forcing runs. The blue hatched patterns in part (c) indicate the region with an altitude >3000 m.
 36 The brown contours in part (d) are the climatological 200 hPa zonal wind (units: m s^{-1}). The
 37 shading shows that at least two-thirds of the members simulate significant changes (at the 95%
 38 significance level), and these significant changes agree on the sign of the average of multiple
 39 members. The black vectors show that for the zonal or meridional component, at least two-thirds
 40 of the members simulate significant changes (at the 95% significance level), and these significant
 41 changes agree on the sign of the average.

42



43

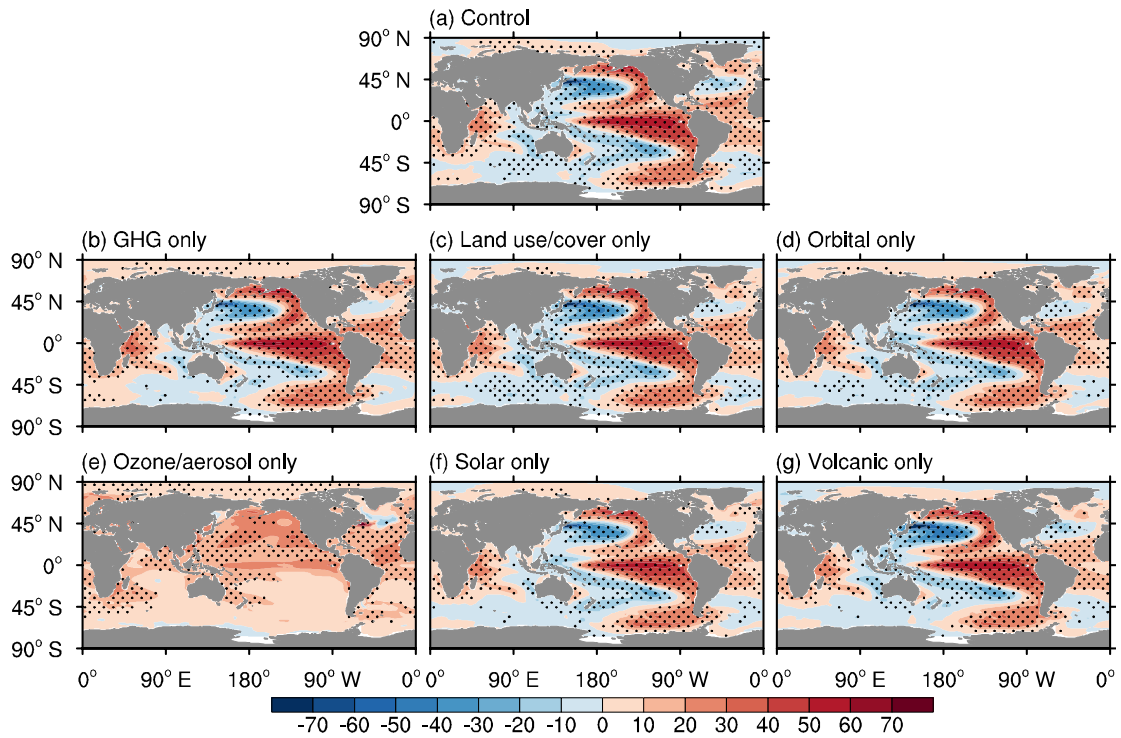
44 **Figure S7.** Simulated autumn atmospheric circulation anomalies during the positive phases of the
 45 IPO. Regressed maps of anomalous (a) vertically integrated water vapor flux from 1000 to 300
 46 hPa (vectors; units: $\text{kg m}^{-1} \text{ s}^{-1}$) and its divergence (shading; units: $10^{-5} \text{ kg m}^{-2} \text{ s}^{-1}$), (b) 500 hPa
 47 vertical velocity (ω_{500}) (units: Pa s^{-1}), (c) 850 hPa wind (uv850) (vectors; units: m s^{-1}) and SLP
 48 (shading; units: hPa), and (d) 500 hPa wind (uv500) (vectors; units: m s^{-1}) and 500 hPa
 49 geopotential height (z500) (shading; units: m) onto the time series of the IPO index simulated by
 50 the CESM-LME all-forcing runs. The blue hatched patterns in part (c) indicate the region with an
 51 altitude >3000 m. The brown contours in part (d) are the climatological 500 hPa geopotential
 52 height (units: m). The shading shows that at least two-thirds of the members simulate significant
 53 changes (at the 95% significance level), and these significant changes agree on the sign of the
 54 average of multiple members. The black vectors show that for the zonal or meridional component,
 55 at least two-thirds of the members simulate significant changes (at the 95% significance level),
 56 and these significant changes agree on the sign of the average.



57

58 **Figure S8.** The leading decadal precipitation mode for the time period 1850–2005 in the
 59 single-forcing simulations. (a–f) The average EOF1 of the nine-year low-pass Lanczos filtered
 60 annual precipitation in six subsets of the single-forcing simulations. The averaged explained
 61 variance is given at the top-right. The shading shows where at least two-thirds of the members
 62 agree on the sign of the average of multiple members.

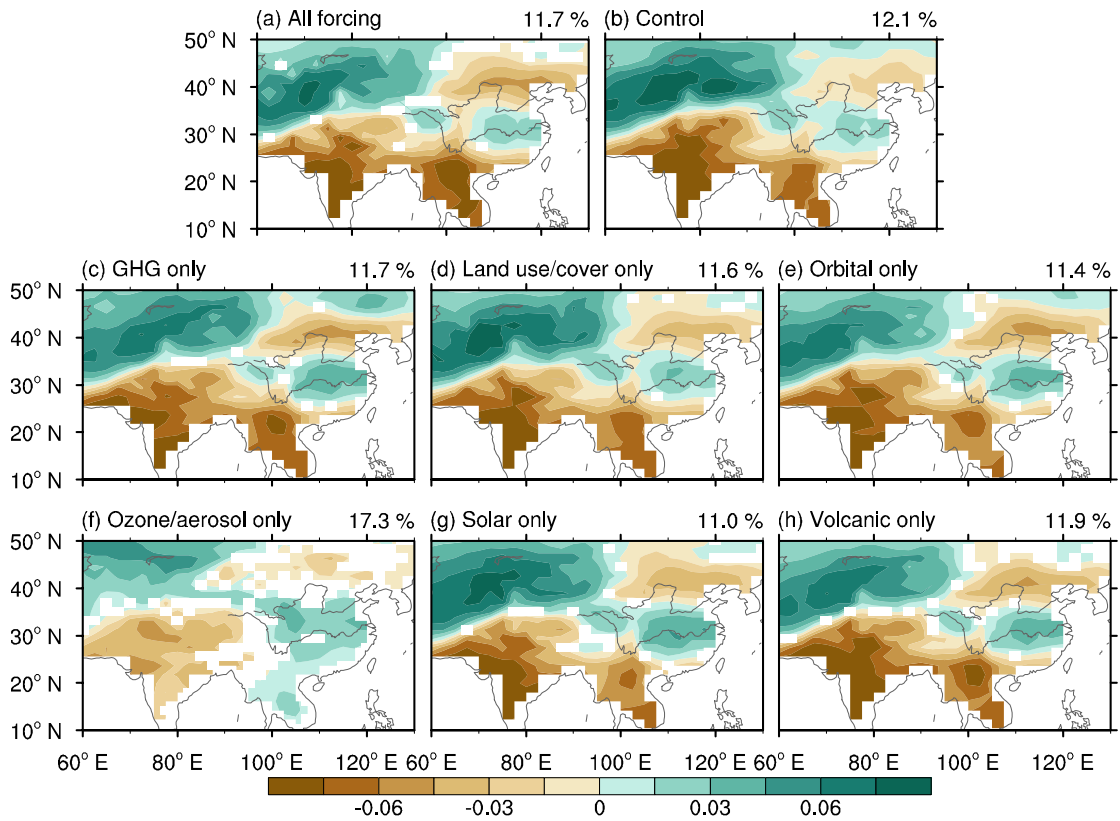
63



64

65 **Figure S9.** The SST anomalies (units: °C) regressed onto the time series of the leading decadal
 66 precipitation mode in the (a) control simulation and (b–g) six subsets of the single-forcing
 67 simulations. The dots in part (a) show significant anomalies at the 95% confidence level and the
 68 dots in parts (b–g) denote that at least two-thirds of the members simulate significant changes (at
 69 the 95% significance level), and these significant changes agree on the sign of the average of
 70 multiple members.

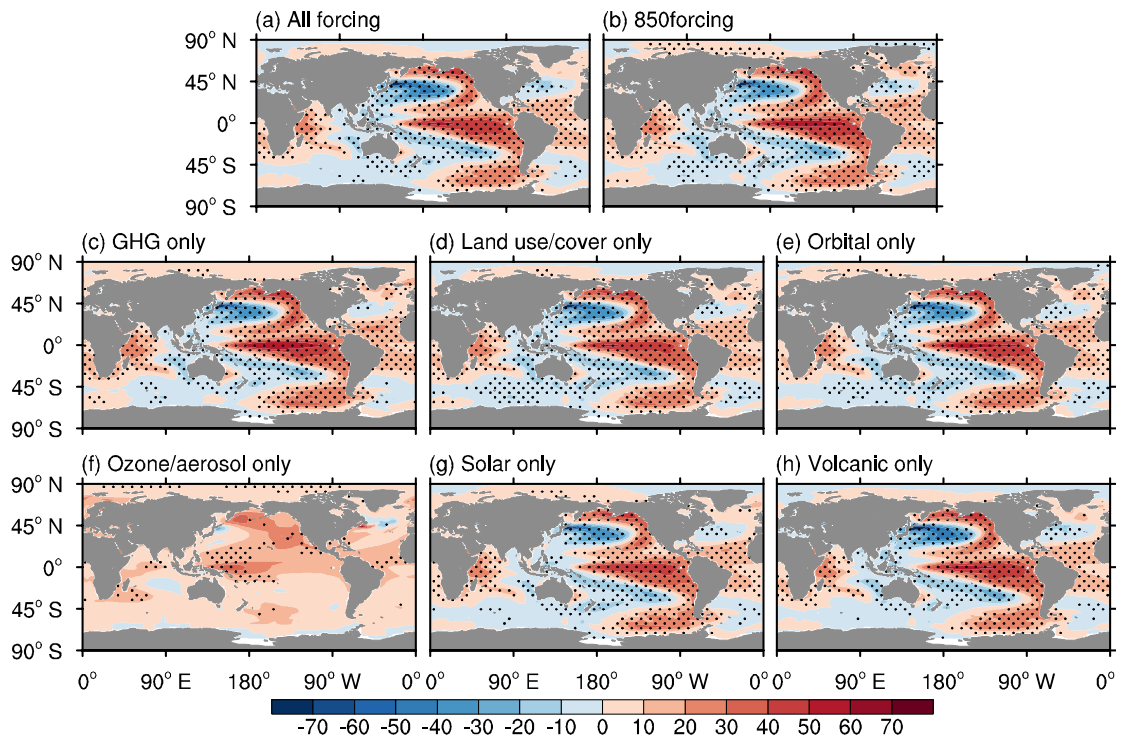
71



72

73 **Figure S10.** The simulated leading decadal soil moisture mode for the time period 850–2005 in all
 74 the experiments, with the exception of leading mode for the time period 1850–2005 in experiment
 75 forced by ozone and aerosols. **(a)** The average EOF1 of the nine-year low-pass Lanczos filtered
 76 soil moisture content (top 10 cm of soil) in the all-forcing simulations. The averaged explained
 77 variance is given at the top-right. **(b)** EOF1 of the nine-year low-pass Lanczos filtered soil
 78 moisture content in the control simulation. The explained variance is given at the top-right. **(c–h)**
 79 The average EOF1 of the nine-year low-pass Lanczos filtered soil moisture content in six subsets
 80 of the single-forcing simulations. The averaged explained variance is given at the top-right. The
 81 shading in parts **(a, c–h)** shows where at least two-thirds of the members agree on the sign of the
 82 average of multiple members.

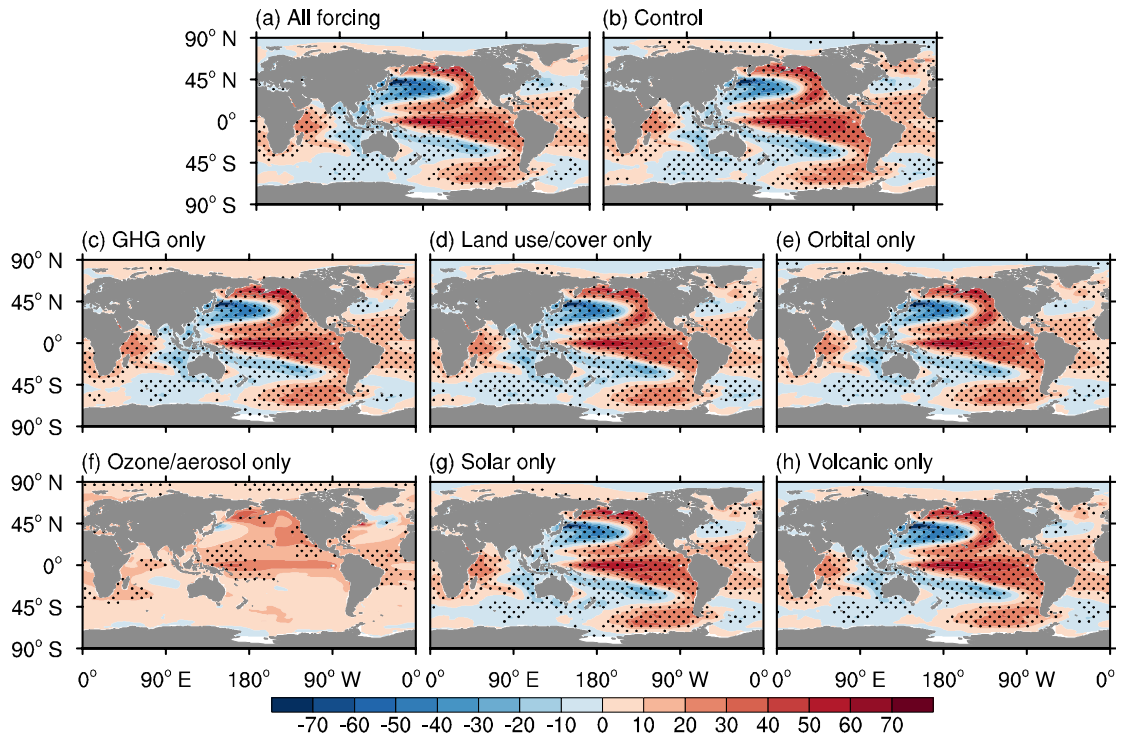
83



84

85 **Figure S11.** The SST anomalies (units: °C) regressed onto the time series of the leading decadal
 86 aridity index mode in the (a) all-forcing simulations, (b) control simulation, and (c–h)
 87 of the single-forcing simulations. The dots in part (b) show significant anomalies at the 95%
 88 confidence level and the dots in parts (a, c–h) denote that at least two-thirds of the members
 89 simulate significant changes (at the 95% significance level), and these significant changes agree
 90 on the sign of the average of multiple members.

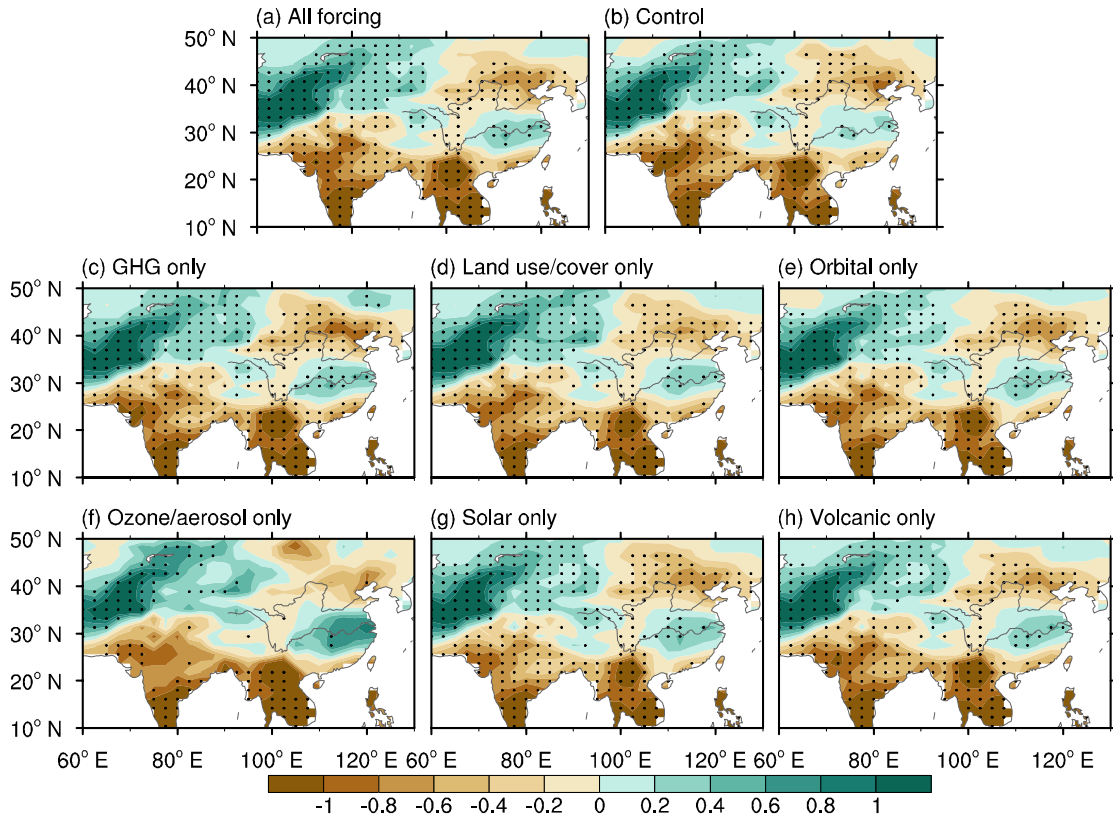
91



92

93 **Figure S12.** The SST anomalies (units: °C) regressed onto the time series of the leading decadal
 94 soil moisture mode in the (a) all-forcing simulations, (b) control simulation, and (c–h)
 95 of the single-forcing simulations. The dots in part (b) show significant anomalies at the 95%
 96 confidence level and the dots in parts (a, c–h) denote that at least two-thirds of the members
 97 simulate significant changes (at the 95% significance level), and these significant changes agree
 98 on the sign of the average of multiple members.

99



100

101 **Figure S13.** Simulated soil moisture anomalies during the positive phases of the IPO. The soil
 102 moisture anomalies (units: kg m^{-2}) regressed onto the time series of the IPO index in the (a)
 103 all-forcing simulations, (b) control simulation, and (c–h) six subsets of the single-forcing
 104 simulations. The dots in part (b) show significant anomalies at the 95% confidence level and the
 105 dots in parts (a, c–h) denote that at least two-thirds of the members simulate significant changes
 106 (at the 95% significance level), and these significant changes agree on the sign of the average of
 107 multiple members.

108

109 **Table S1.** The correlations across the time series of the leading decadal precipitation mode
 110 simulated by CESM-LME 12 all-forcing simulations.

Cor	#002	#003	#004	#005	#006	#007	#008	#009	#010	#011	#012	#013
#002	1.00	—	—	—	—	—	—	—	—	—	—	—
#003	0.10	1.00	—	—	—	—	—	—	—	—	—	—
#004	0.14	0.15	1.00	—	—	—	—	—	—	—	—	—
#005	0.17	0.17	0.19	1.00	—	—	—	—	—	—	—	—
#006	0.16	0.14	0.16	0.11	1.00	—	—	—	—	—	—	—
#007	0.16	0.17	0.20	0.21	0.19	1.00	—	—	—	—	—	—
#008	0.20	0.19	0.26*	0.24*	0.18	0.25*	1.00	—	—	—	—	—
#009	0.12	0.14	0.15	0.11	0.08	0.12	0.22*	1.00	—	—	—	—
#010	0.16	0.19	0.26*	0.23*	0.12	0.31*	0.35*	0.08	1.00	—	—	—
#011	0.03	0.19	0.24*	0.16	0.16	0.12	0.17	0.10	0.16	1.00	—	—
#012	-0.06	0.04	0.01	0.02	-0.06	-0.02	-0.02	0.05	0.04	0.04	1.00	—
#013	0.09	0.08	0.15	0.20	0.05	0.16	0.11	0.03	0.14	0.09	0.07	1.00

111 * denotes significant correlation at the 95% confidence level, except for autocorrelations.

112